2-18-2004

Kuroshio Intrusion and the Circulation in the South China Sea

H. J. Xue

Fei Chai
University of Maine - Main, fchai@maine.edu

Neal Pettigrew
University of Maine - Main, nealp@maine.edu

D. Y. Xu

M. Shi

See next page for additional authors

Kuroshio intrusion and the circulation in the South China Sea

Huijie Xue, Fei Chai, Neal Pettigrew, and Danya Xu
School of Marine Sciences, University of Maine, Orono, Maine, USA

Maochong Shi
Ocean University of China, Qingdao, China

Jianping Xu
Second Institute of Oceanography, Hangzhou, China

Received 23 November 2002; revised 2 October 2003; accepted 19 November 2003; published 18 February 2004.

[1] The Princeton Ocean Model is used to study the circulation in the South China Sea (SCS) and its seasonal transition. Kuroshio enters (leaves) the SCS through the southern (northern) portion of the Luzon Strait. The annually averaged net volume flux through the Luzon Strait is ~2 Sv into the SCS with seasonal reversals. The inflow season is from May to January with the maximum intrusion of Kuroshio water reaching the western SCS during fall in compensation of summertime surface offshore transport associated with coastal upwelling. From February to April the net transport reverses from the SCS to the Pacific. The intruded Kuroshio often forms an anticyclonic current loop west of the Luzon Strait. The current loop separates near the Dongsha Islands with the northward branch continuously feeding the South China Sea Warm Current (SCSWC) near the shelf break and the westward branch becoming the South China Sea Branch of Kuroshio on the slope, which is most apparent in the fall. The SCSWC appears from December to February on the seaward side of the shelf break, flowing eastward against the prevailing wind. Diagnosis shows that the onshore Ekman transport due to northeasterly monsoon generates upwelling when moving upslope, and the particular distributions of the density and sea level associated with the cross shelf motion supports the SCSWC. *INDEX TERMS:* 4532 Oceanography: Physical: General circulation; 4255 Oceanography: General: Numerical modeling; 4243 Oceanography: General: Marginal and semienclosed seas; *KEYWORDS:* South China Sea, circulation, Kuroshio

Citation: Xue, H., F. Chai, N. Pettigrew, D. Xu, M. Shi, and J. Xu (2004), Kuroshio intrusion and the circulation in the South China Sea, *J. Geophys. Res.*, *109*, C02017, doi:10.1029/2002JC001724.

1. Introduction

[2] The South China Sea (SCS) is a large tropical marginal sea that extends from the equator to 23°N and from 99° to 120°E (Figure 1). It plays a significant role in the formation of Southeast Asian Monsoon that affects all the bordering countries [*Lau and Lau*, 1992]. The SCS is connected to the East China Sea, the Java Sea, and the Indian Ocean via a labyrinth of narrow and shallow sea straits. In contrast, its connection to the western Pacific through the Luzon Strait is deep and wide. Even though the deepest part of the SCS exceeds 5000 m, the exchange below the 200-m isobath occurs only in the Luzon Strait which gives rise to its semienclosed nature. Continental shelves are wide in the northern and southwestern SCS, but extremely narrow in the east and west.

[3] The SCS is subjected to the strong forcing of alternating northeast and southwest monsoon winds, frequent typhoons, seasonal incursions of the Kuroshio Current, and fresh water inflows from the Pearl River and the Mekong River. Its large size, low latitude, and semienclosed nature add additional dynamical complexity that foretells of convergent shelf and coastal currents that may in turn engender counter currents, undercurrents and gyres in the shelf/slope region.

[4] Because of the paucity of direct current measurements, many of the prevailing notions about the SCS circulation are derived from a combination of hydrographic distributions and modeling results [e.g., *Wyrtki*, 1961; *Nitani*, 1972; *Li et al.*, 1994; *Shaw and Chao*, 1994; *Metzger and Hurlburt*, 1996; *Xu and Su*, 1997; *Fang et al.*, 1998; *Chu et al.*, 1999; *Wu et al.*, 1999; *Chu and Li*, 2000; *Qu*, 2000; *Qu et al.*, 2000; *Metzger and Hurlburt*, 2001]. *Hu et al.* [2000] compiled an extensive review on the currents in the SCS and summarized that (1) the seasonal SCS circulation is mostly driven by the monsoon winds such that the upper layer (0 ~ 200 m) mean circulation is cyclonic in winter but changes to anticyclonic in summer; (2) the circulation in the northern SCS is closely related to the inflows and outflows through the Luzon and the Taiwan

0148-0227/04/2002JC001724

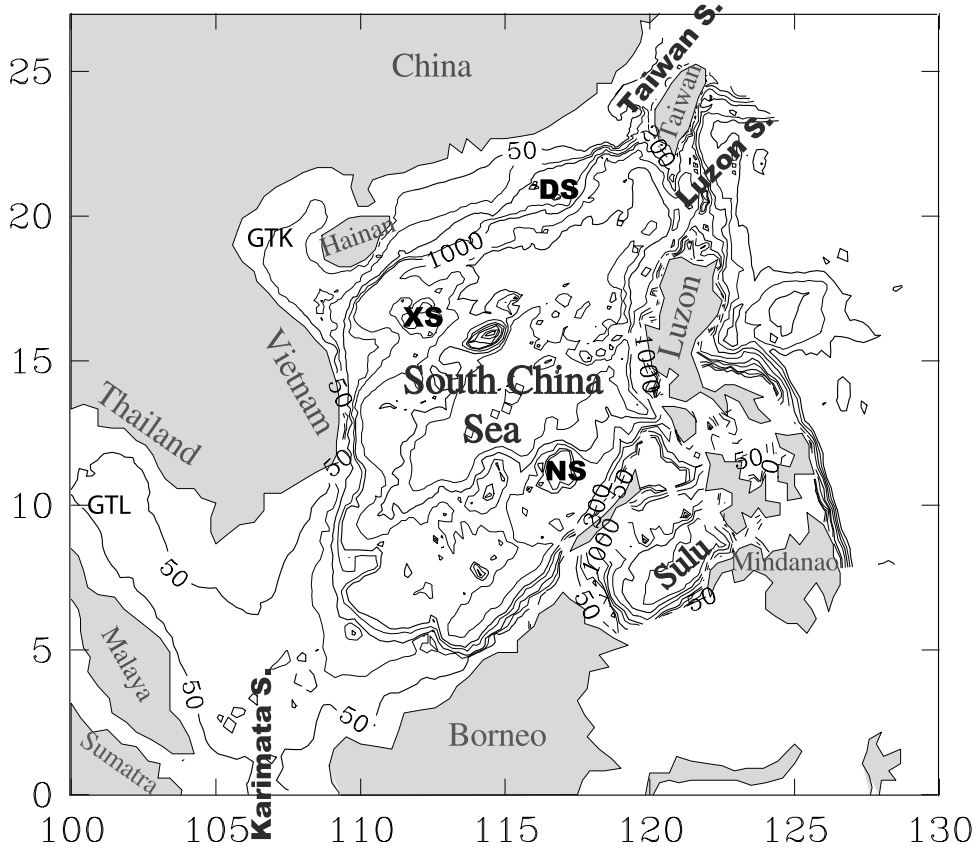

Figure 1. Topography of the SCS and the neighboring Sulu Sea and Philippine Sea. Contours are the 50-, 100-, 200-, 600-, 1000-, 2000-, 3000-, 4000-, and 5000-m isobaths, respectively. DS, Dongsha Islands; XS, Xisha Islands; NS, Nansha Islands; GTK, Gulf of Tonkin; and GTL, Gulf of Thailand.

Strait; and (3) several cyclonic eddies have been noted repeatedly, two in winter occurring west of Luzon Island and southeast of the Vietnam Peninsula and one in summer off the Vietnam coast.

[5] *Nitani* [1972] first showed the intrusion of the Kuroshio as an anticyclonic current loop in the SCS. With the aid of satellite AVHRR and altimetry, *Fang et al.* [1998] suggested that the Kuroshio intrusion after entering the SCS splits into three parts. A major part flows out the SCS through the northern section of the Luzon Strait and forms an anticyclonic current loop west of the Luzon Strait, the second part extends westward on the northern slope, also known as the South China Sea Branch of Kuroshio (SCSBK), and the third feeds the cyclonic eddy west of Luzon (Figure 2). The current loop has a large range in winter but it is smaller in summer. It provides a source of warm water for the South China Sea Warm Current (SCSWC) and the Taiwan Warm Current (TWC) [*Shaw*, 1991].

[6] The SCSWC appears as an intermittent northeastward current along the shelf break of the northern SCS, spanning from the southeast of Hainan Island to the southwest of Taiwan. The current can be as wide as 160–300 km with the maximum surface speed of 30 cm s^{-1} [*Guan*, 1978, 1985]. The most striking feature of the SCSWC is that it flows against the wind in winter. Several mechanisms have been proposed to explain the formation of the SCSWC. For example, *Chao et al.* [1995] suggested that northeasterly winds result in a sea level buildup along the northwestern boundary of the SCS and the subsequent relaxation of the wind triggers a returning current on the shelf. The northeastward current in their model appears to be strongest east of the Hainan Island and weakens gradually toward east. *Zhong* [2001] proposed that the alongshore pressure gradient imposed at the shelf break drives a northeastward warm current in accordance with the arrested topographic wave theory of *Csanady* [1978]. *Li et al.* [1998] speculated that the SCSWC is perhaps the northern portion of the anticyclonic current loop or an anticyclonic warm core ring that might have been separated from the current loop. For example, a warm core ring of Kuroshio origin was observed during the research cruise in September 1994. It was centered at about 117.5°E, 21°N on the northern slope of the SCS [*Li et al.*, 1998].

[7] Results from the recent model of *Metzger and Hurlburt* [2001] indicate that the Kuroshio penetration has no tangible relation with the transport through the Luzon Strait, and that its variability can be attributed to the nondeterministic mesoscale flow instabilities. As calculated by the model, the transport through the Luzon Strait is from the Pacific to the South China Sea varying from a low of 1.0 Sv in December–January–February to a high of 3.2 Sv in June–July–August. Geostrophic calculation by *Qu* [2000], on the other hand, shows a seasonal Luzon Strait transport with maximum of 5.3 Sv in January–February and minimum of 0.2 Sv in June–July, which is consistent with

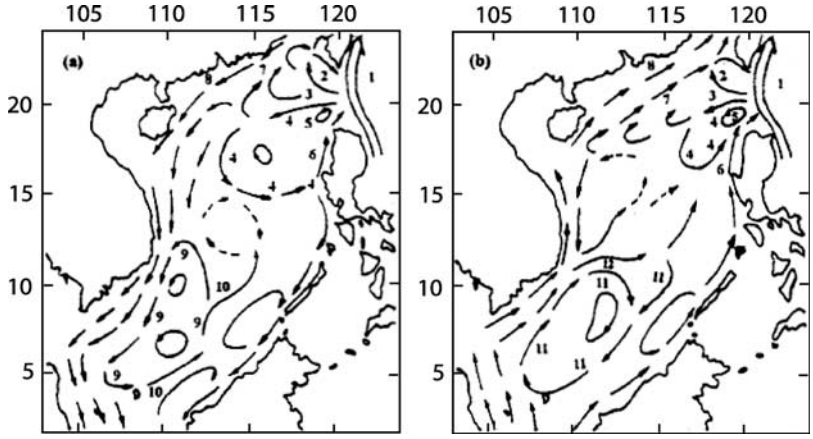

Figure 2. Schematic of the SCS circulation in (a) winter and (b) summer: 1, Kuroshio; 2,current loop; 3, SCSBK; 4, Luzon cyclonic gyre; 5, Luzon cyclonic eddy; 6, Luzon coastal current; 7, SCSWC; 8, Guangdong Coastal Current; 9, SCS southern cyclonic gyre; 10, Natuna offshelf current; 11, SCS southern anticyclonic gyre; and 12, Vietnam offshore current. After *Fang et al.* [1998].

the hypothesis that the Kuroshio intrusion is driven by the northeast monsoon in winter [*Farris and Wimbush*, 1996]. It is interesting though that salinity on the northern slope appears to vary semiannually with high in summer and winter, and low in spring and fall [*Qu et al.*, 2000]. The increase of salinity from spring to summer is difficult to explain since the Luzon Strait transport is low at the time of the year. *Qu* [2000] tried to distinguish the difference between the Luzon Strait transport and the intruded Kuroshio water found along the continental slope south of China, and attributed the latter to the pressure gradient along the slope that has a semiannual variation.

[8] While the previous studies have stimulated a great deal of interest and raised important questions, direct current measurements are scarce and the models have not been of sufficient resolution to adequately treat the complex circulation features in the northeastern SCS. Furthermore, most of the models neglect the exchange with the Sulu Sea and often prescribe the transport at the Luzon Strait. On the other hand, the Pacific basin-scale models of *Metzger and Hurlburt* [1996, 2001] omit the continental shelf region where the water depth is less than 200 m. Estimates of the annual mean Luzon Strait transport vary greatly in the literature, ranging from 0.2 [*Wyrtki*, 1961] to 4.2 Sv [*Qu et al.*, 2000]. Given the complex inflow-outflow patterns observed [*Xu and Su*, 1997], sufficient resolution is needed to quantify the net transport through the Luzon Strait. In this study, the model domain is extended to include a small area of the western Pacific Ocean and the entire Sulu Sea, hence fewer constraints are imposed on the exchange between the SCS and the neighboring regions, especially the excursion/incursion of the Kuroshio through the Luzon Strait. The modeled general circulation for the upper SCS is described in section 3. Kuroshio intrusion through the Luzon Strait, its relation to the circulation in the northern SCS, and the presence of the SCSBK on the northern slope during the fall are discussed in section 4. A seasonal mass balance in the SCS is inferred on the basis of the model results. In addition, the present model has finer resolution in the northern SCS, adequate to resolve mesoscale eddies and other prominent circulation features there. Results from the model are used in diagnosis of the dynamic balance associated with the SCSWC.

2. Model Setup

[9] The three-dimensional Princeton Ocean Model [*Blumberg and Mellor*, 1987] is configured for the SCS in an orthogonal curvilinear coordinate with a total of 151 × 101 grid points (Figure 3). It has variable grid sizes. The finest resolution is in the northern shelf of the SCS where

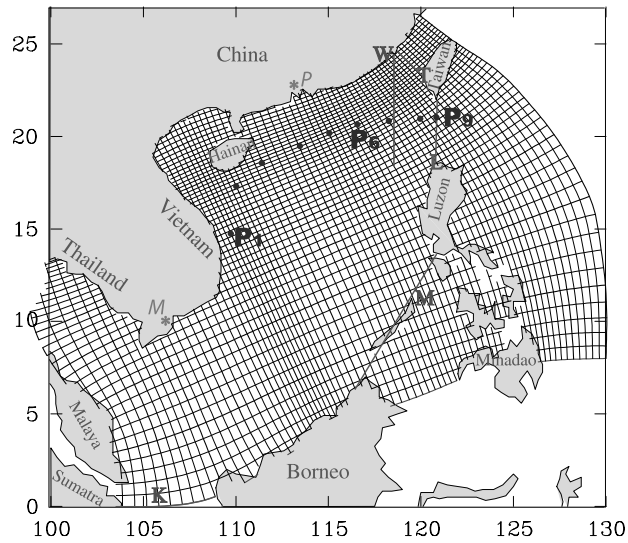

Figure 3. Horizontal grid of the SCS circulation model at the half resolution. Cross sections T, L, M, and K enclose an area referred as the SCS in this paper. Transports across the sections T and L are shown in Figure 4a. Two major estuaries (P, Pearl River, and MK, Mekong River) are marked with asterisks. The dots follow approximately the 300-m isobath in the model from Vietnam coast (P_1) to southwest of Dongsha (P_6). From P_6 eastward to P_9 in the Luzon Strait the dots cut across the anticyclonic current loop. The cross section W is used to illustrate the SCSWC.

Table 1. Monthly Pearl River Discharge as Percentages of the Annual Discharge[a]

Month	Percent
1	2.9
2	2.8
3	3.4
4	7.0
5	13.9
6	13.7
7	17.2
8	14.4
9	9.2
10	6.7
11	4.9
12	3.9

[a]From *Zhao* [1990].

grid size ranges from 9 km at the coast to about 12 km at the shelf break. Resolution is also relatively high off the coasts of Vietnam and Philippines. The model has 22 sigma levels in the vertical with higher resolution in both the surface and the bottom boundary layer. The ETOPO5 data set is used to specify the bottom topography with the maximum depth set to 6000 m in the model.

[10] At the surface, the model is forced with monthly climatological winds and net heat and freshwater fluxes from the Comprehensive Ocean Atmosphere Data Set (COADS). The SCS is under the strong and sometimes simultaneous influence of both the Southeast Asian and Indian Monsoon systems. Climatological data suggest that the winter northeast monsoon ends in April, and that winds in the region are generally weak during this time of year. The southwest monsoon first appears in the central basin in May and expands over the entire basin in July and August. The transition from summer to winter is characterized by the gradual southward advancement of northeast monsoon conditions. The northeast monsoon first appears over the northern shelf in October, at which time the southwest monsoon still prevails in the south. This convergent wind pattern, due to the great size of the SCS, strongly influences the circulation in the SCS. The northeast monsoon subsequently expands southward against the diminishing southwest monsoon during October and November, reaching its maximum in December and covering the entire SCS.

[11] In addition to the winds, monsoons also bring excessive precipitation to the region with an annual averaged rainfall of 2 m. The resultant freshwater runoff into the SCS, especially from the Pearl River in the north and the Mekong River in the southwest, is large even by global standards and plays an important role in the hydrographic and flow regimes on the shelf. *Perry et al.* [1996] estimated the annual averaged discharge rate at 15,000 and 10,000 $m^3 s^{-1}$ for the Mekong River and the Pearl River, respectively. In the model, discharge from both rivers varies from month to month according to the percentages given in Table 1.

[12] There are two open boundaries in the model. To the east, the model is connected with the East China Sea (Taiwan Strait) and the western Pacific Ocean. To the south, the model is connected with the Java Sea (Karimata), the Celebes Sea (channels through Sulu Archipelagos), and the Pacific Ocean. The monthly climatology obtained from the 10-year simulation of the Navy Postgraduate School ¼° × ¼° Parallel Ocean Climate Model (POCM) from 1988 to 1997, with linear interpolation between months, is specified at these two open boundaries.

[13] Specifically, the sea level and the vertically averaged velocity perpendicular to the boundary from the POCM are incorporated in the open boundary condition for the normal barotropic velocity in the form of $H\overline{U} - c_e\eta = \left(H\overline{U} - c_e\eta\right)_{BC}$. For the 3-D variables, gravity wave radiation combined with three-point smoothing is applied to the baroclinic velocity normal to the boundary, while the upwind advection is applied to the temperature and salinity such that the monthly POCM temperature and salinity are carried into the domain in case of inflows.

[14] After initialized with the POCM 10-year averaged January condition, the model is then integrated forward in time with monthly forcing for 20 years. Output from the model are averaged every 5 days and then archived. Figure 4a shows the transport through the southern Taiwan Strait (see section T in Figure 3) and the Luzon Strait (see section L in Figure 3), and Figure 4b shows the kinetic energy in the SCS throughout the 20-year model integration. It appears that shallow areas have reached equilibrium such that the transport through the Taiwan Strait has attained a steady annual cycle (Figure 4a). There is a low-frequency modulation in the transport through the Luzon Strait since a large portion of the channel is deeper than 1000 m, suggesting a longer integration period is needed for the deep SCS to reach equilibrium. The total kinetic energy in the SCS (defined here as the area enclosed by the cross

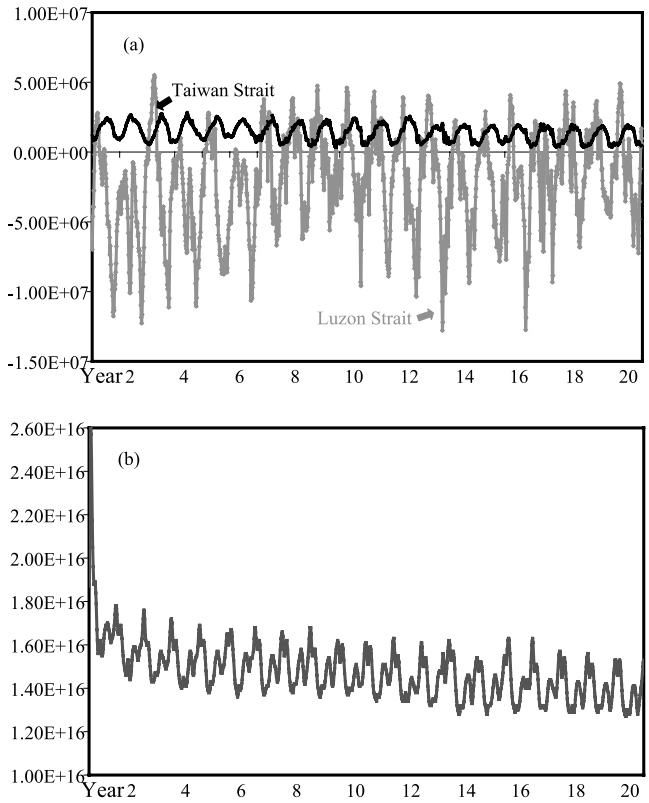

Figure 4. Time series of (a) the transport through the Taiwan Strait and the Luzon Strait and (b) the total kinetic energy in the SCS.

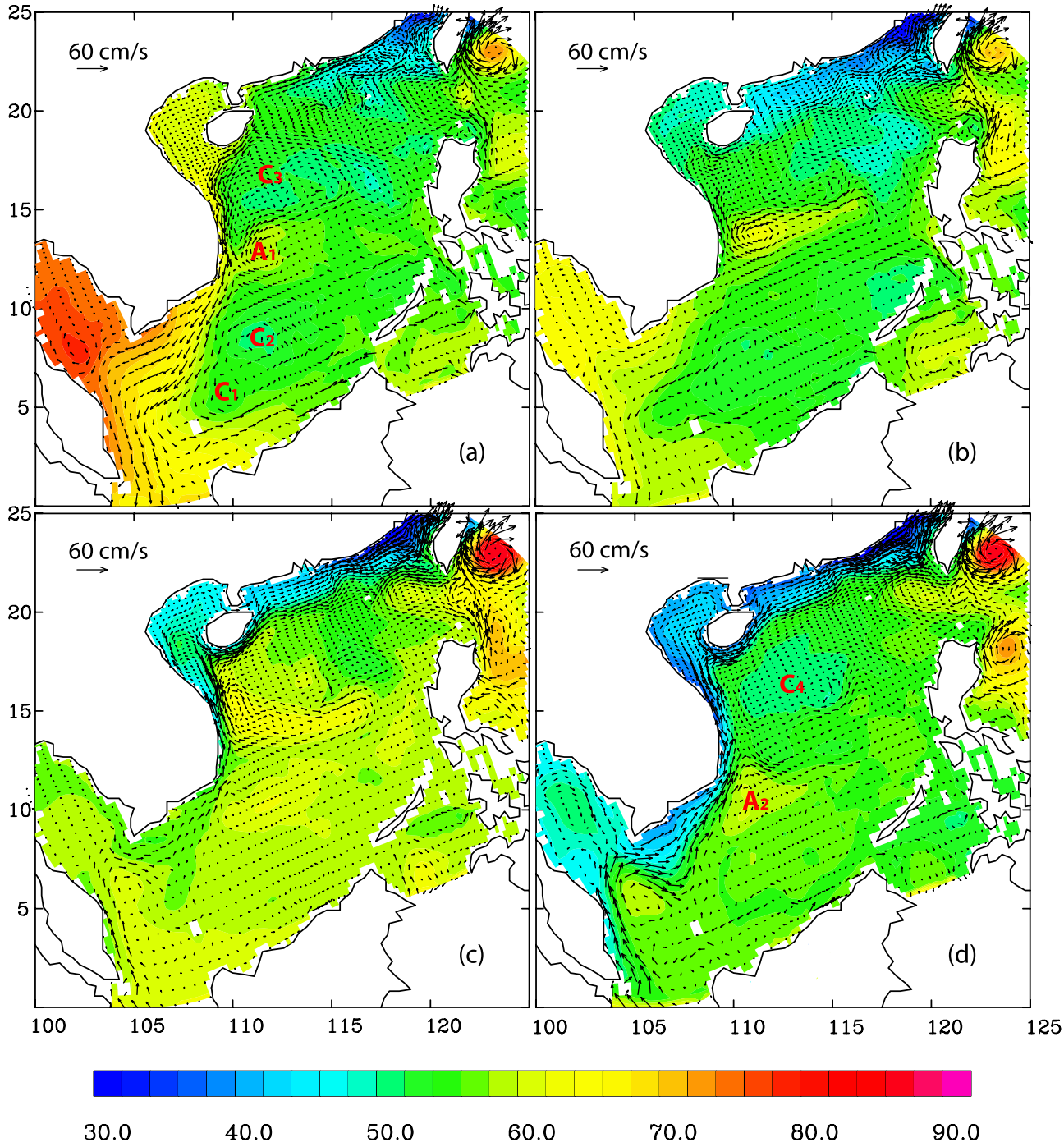

Figure 5. Sea surface elevation and the upper layer flow patterns vertically averaged in the top 200 m: (a) January, (b) March, (c) May, (d) July, (e) September, and (f) November. The unit for sea surface elevation is cm.

sections T, L, M, and K shown in Figure 3) has been slowly approaching a steady annual cycle.

3. Seasonal Circulation in the SCS

[15] The archived model results from the last 6 years have been processed to obtain monthly averaged temperature, salinity, velocity, and sea level, from which one can examine the seasonal circulation pattern emerged from this simulation. To compare with the schematic of *Fang et al.* [1998], velocity field is averaged in the top 200 m to illustrate the upper layer circulation, which is shown in Figure 5 along with the corresponding sea surface elevation.

[16] The simulated upper ocean circulation pattern agrees rather well with the schematic patterns of *Fang et al.* [1998] for both summer and winter. In winter (Figure 5a), the combination of the wind-driven and gradient forcing results in a southwestward and southward coastal current system

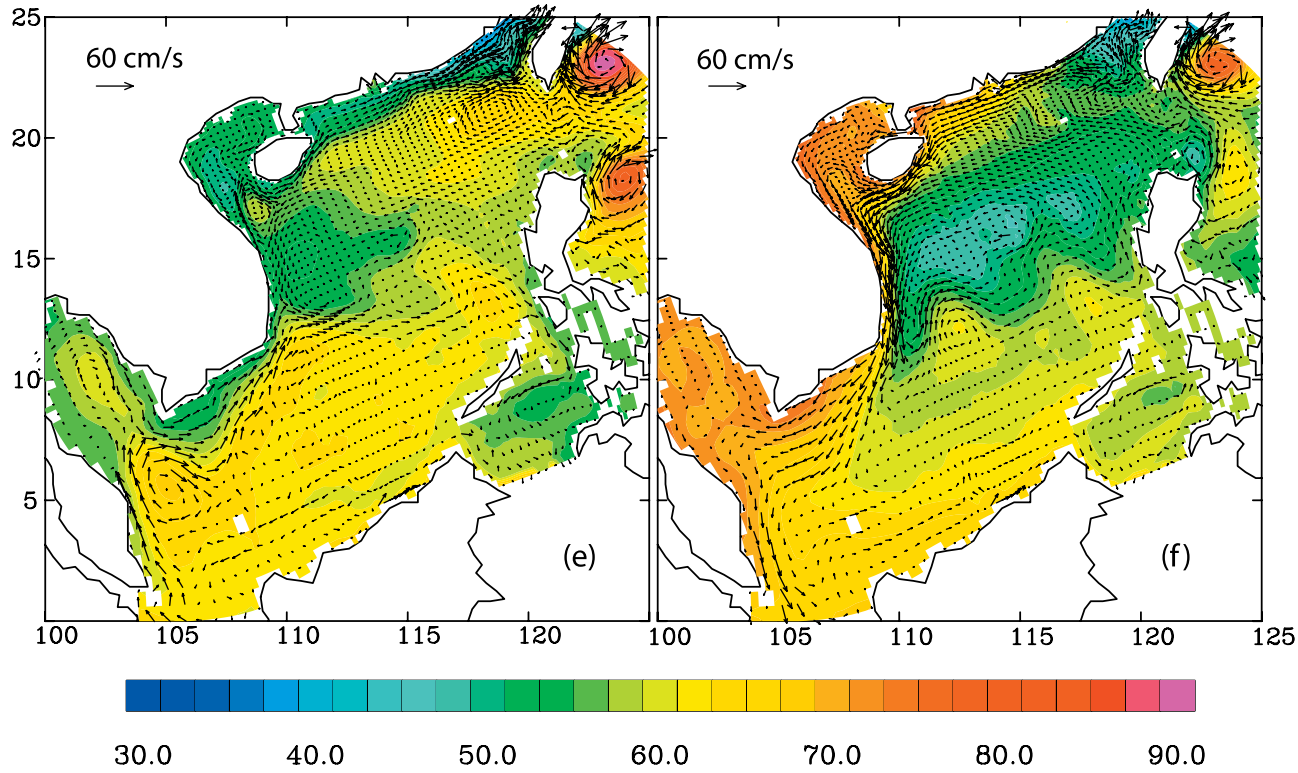

Figure 5. (continued)

off the coasts of China and Vietnam. Part of the cyclonic circulation leaves the SCS through the Karimata Strait, and the rest moves northeastward along the Borneo slope continuing the cyclonic motion. An intermittent southwestward flow occurs right next to the Borneo coast forming two elongated anticyclonic eddies there. In the interior basin, one cyclonic eddy (C_1) occurs at the very southwest corner and another (C_2) slightly to the northeast of C_1. Both eddies are encompassed by a cyclonic gyre in the southern basin between ~5° and ~12°N. There is also a cyclonic gyre (C_3) in the northern basin between 15° and 19°N. Between these two cyclonic gyres, circulation is generally anticyclonic. In particular, there appears an anticyclonic eddy (A_1) east of Vietnam center at 111°E and 13°N. The presence of A_1 has also been detected in the 1998 shipboard ADCP measurements [*Shi et al.*, 2001]. In summer (Figure 5d), the circulation in the southern basin turns anticyclonic. Part of the northward Vietnam Coastal Current separates from the coast around 12°N and flows eastward. To the north of the eastward current, there exists a cyclonic gyre (C_4) in the deep basin of the northwestern SCS.

[17] The surface elevation in the SCS behaves like an asymmetric seesaw with larger annual oscillation on the west and smaller one on the east. The maximum annual variation of sea level occurs in the Gulf of Thailand where the difference between the high in winter and the low in summer is about 40 cm. Ekman transport associated with the northeasterly monsoon results in water pileup first in the northwest corner around the Gulf of Tonkin in November. The high sea level then extends southward from fall to winter as the northeasterly monsoon strengthens and advances southward. The situation reverses during summer when southwesterly monsoon drives an offshore water movement along the western and northern coasts of the SCS hence the sea level is low and there are strong upwellings associated with the offshore Ekman transport along the Vietnam and southern China coasts as discussed by *Xue et al.* [2000]. As well, the coastal sea level low appears first in the north and then extends southward from March to July. As a result, the change of the coastal currents from south-southwestward to north-northeastward also appears first in the northern SCS (Figure 5b). It is speculated that the receding winter monsoon and the presence of an area of high sea level in the central basin (Figure 5b) triggers the current reversal in the north, which is later reinforced throughout the SCS as the summertime southwesterly monsoon begins to take over in May.

[18] To illustrate clearly the sea level pattern over the interior basins and compare the model result with altimeter data, Figure 6 shows the anomaly of the modeled surface elevation inside the 1000-m isobath in a 2-month increment starting February. The anomaly is obtained by subtracting the domain-averaged elevation of the corresponding month. In the interior basins of the SCS, a high develops off the central Vietnam coast during winter (Figure 6a), in contrast to the low west of the Luzon Island and the low in the southern basin. The high and the low west of Luzon continue to strengthen from February to April. Meanwhile the high associated with the Kuroshio begins to move into the SCS and gradually strengthens throughout the summer (Figures 6b, 6c, and 6d). From April to August, The high east of the Vietnam, the low west of Luzon Island, and the high near the Luzon Strait all migrate south or westward along the rim of the deep basin. By October (see Figure 6e), the sea level is relatively high in the southern half of the SCS but low in the northwestern interior basin. However,

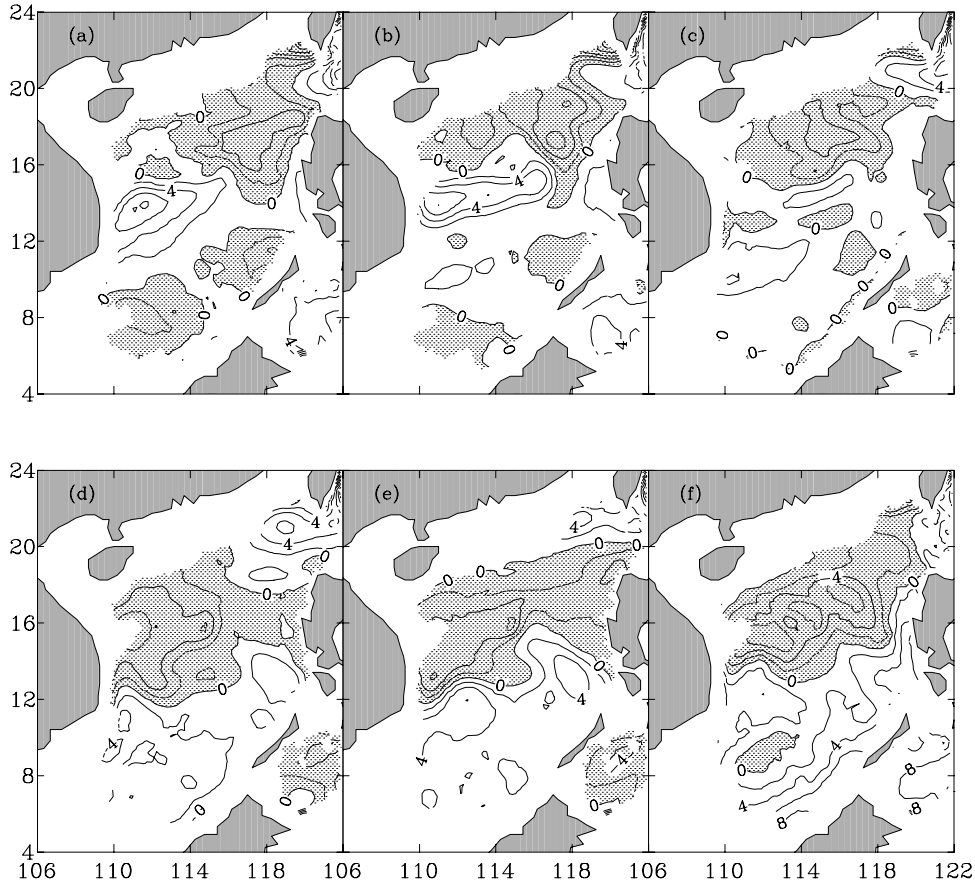

Figure 6. Sea surface elevation anomaly (with the domain average subtracted) in the deep basins of the South China Sea in (a) February, (b) April, (c) June, (d) August, (e) October, and (f) December. Contour interval is 2 cm. Areas with negative anomaly are shaded.

the high associated with the intruded Kuroshio extends westward across the northern slope. During the fall-to-winter transition in November, the low expands over the interior basins and strengthens especially in the north. This may be related to the fact that during the transition period the southwesterly monsoon is still present over the southern SCS while the northeasterly monsoon arrives in the north. The expansion and strengthening of the low in the north cut off the high sea level band on the northern slope and push the high sea level toward the Gulf of Tonkin.

[19] The aforementioned spatial and temporal patterns of the sea surface elevation compare favorably with the altimeter data shown by *Wu et al.* [1999] and *Liu et al* [2001]. The only disagreement appears during summer in the northern basin where although the modeled low continues to weaken and drifts westward the high from the Luzon Strait has not established (Figure 6c), whereas in the altimeter data the high from the Luzon Strait joins with the southern high to dominate the northern and the western part of the interior basins. In general, the evolution of the sea surface elevation can be attributed to the changing wind field. Except in the vicinity of the Luzon Strait where the Kuroshio intrusion is dynamically important as pointed out by *Metzger and Hurlburt* [2001], the sea surface elevation responds to the wind stress curl (Figure 7) such that the high in sea level corresponds with the negative wind stress curl and vice versa). Analysis of the dynamic height in the SCS by *Qu* [2000] suggested also that the formation of cyclonic or anticyclonic gyres is determined by wind stress curl, more so in the eastern part than in the western part.

4. Kuroshio Intrusion and the Circulation in the Northern SCS

[20] Kuroshio intrusion through the Luzon Strait and the westward movement of the Kuroshio water on the northern slope of the SCS were observed by *Guo et al* [1985], *Li and Wu* [1989], and *Xu and Su* [1997]. In particular, *Xu and Su* [1997] depicted three pairs of interleaving inflows and outflows in the Luzon Strait on the basis of the hydrographic data collected during the survey in August–September 1994. Moreover, *Shaw* [1991] analyzed the SCS hydrographic station data in the National Oceanographic Data Center archive and showed that the Philippine Seawater was present along the entire northern slope between the 200- and 1000-m isobaths from October to January, whereas from February to September the Philippine Seawater was located in the vicinity of the Luzon Strait. To illustrate the complex spatial and temporal variability of the inflows and outflows in the Luzon Strait, monthly averaged velocities from the model are interpolated to the section L at 56 z levels. They are then decomposed in the directions tangential and per-

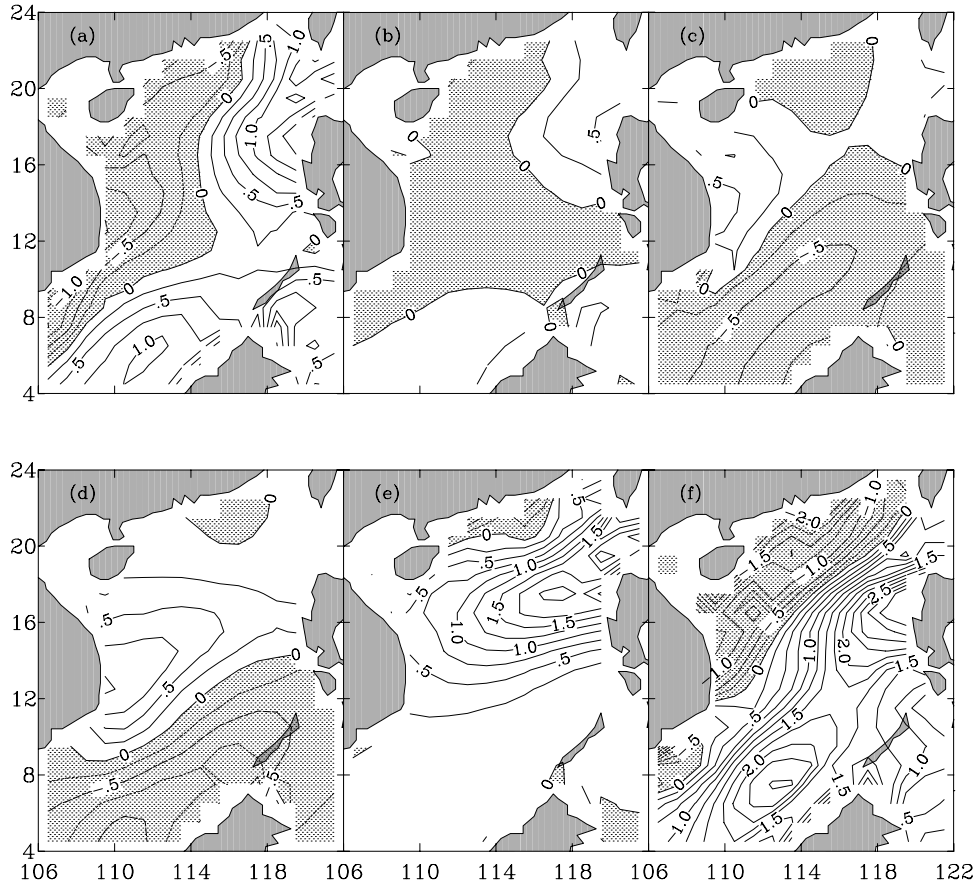

Figure 7. Wind stress curl ($\times 10^{-7}$ N m^{-3}) from the COADS in (a) February, (b) April, (c) June, (d) August, (e) October, and (f) December. Contour interval is 0.25×10^{-7} N m^{-3}. Areas with negative wind stress curl are shaded.

pendicular to the section, from which the net transport through the Luzon strait is calculated.

4.1. Transport Through the Luzon Strait

[21] Net transport through the Luzon Strait (T_L) shown in Figure 8 exhibits remarkable seasonal variation. It is from the Pacific into the SCS during most time of the year except that between February and April it is from the SCS to the Pacific. The annual mean transport of 2.0 Sv is rather close to the estimate of *Metzger and Hurlburt* [2001]. The maximum inflow, however, occurs later in this study in September–October as oppose to June–July–August in *Metzger and Hurlburt* [2001]. Since there is no obvious relationship between the Luzon Strait transport and the prevailing monsoon, another possible explanation is that the mass balance within the SCS allows more water to flow into the region in the fall. To investigate, temporal change of the elevation along the northern slope is extracted from the model results (Figure 9). From January to June, surface elevation is higher on both ends (i.e., the Vietnam coast (P_1) and the Luzon Strait (P_9)) but low southwest of Dongsha (P_6). Especially starting from March, sea level begins to build up in the Luzon Strait. However, the sea level high in the northwest SCS and the associated anticyclonic circulation in April and May (shown in Figure 5c) impede any possible westward penetration. Most of the intrusion has to return to the Pacific (more discussion in section 4c), resulting in a small net T_L. Starting in July, sea level drops in the western SCS, surface elevation decreases monotonically from east (P_9) to west (P_1). This appears to induce another burst of Kuroshio intrusion in the Luzon Strait. Without the impediment from the western SCS at this time, the intrusion is able to penetrate deep into the SCS across the entire northern slope. From the lowest sea level near the Vietnam coast in July–August to the maximum inward transport in

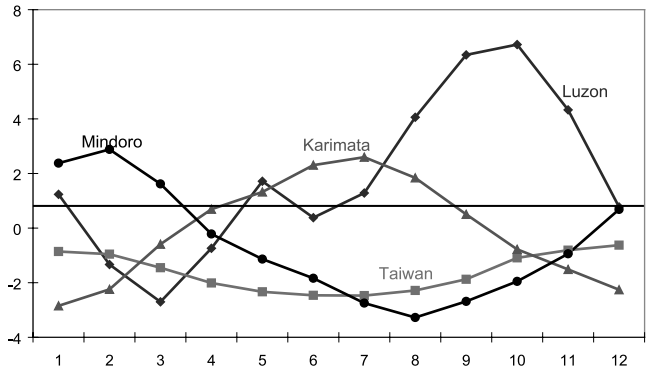

Figure 8. The 6-year averaged monthly transport of flows entering (positive) and leaving (negative) the South China Sea through the Luzon (diamond), Taiwan (square), Karimata (triangle), and Mindoro (solid circle) Strait.

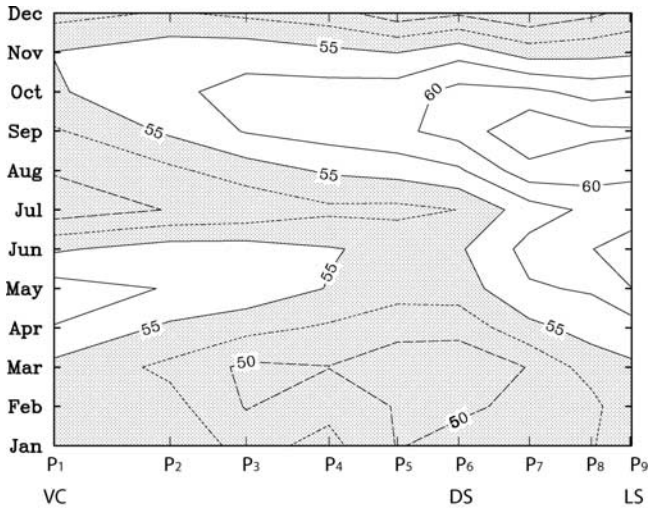

Figure 9. Seasonal variation of the sea surface elevation along the northern slope in the SCS. See Figure 3 for locations of P_i, i = 1, 2, . . ., 9. P_1 is located near the Vietnam coast, P_6 is located southwest of Dongsha, and P_9 is in the Luzon Strait. Contour interval is 2.5 cm. Shaded areas have elevation below 55 cm.

the Luzon Strait, the time lag is about two months. Furthermore, it takes about another two month for the high elevation signal from the Luzon Strait to reach Vietnam coast.

[22] The net transport through the Luzon Strait with an annual mean of ~2.0 Sv from the Pacific to the SCS plays an important role in the SCS water mass balance. It represents the single largest source of water import into the SCS. The net transport through the Taiwan Strait (T_T), however, represents the largest export of water for the SCS, being northward year-round with the maximum in summer (Figure 8). Although T_T is calculated using a section near the southern end of the Taiwan Strait (see Figure 3), it is still constrained by the open boundary condition imposed at the northern end of the strait. Despite that the integrated transport is northward year-round, there is a southward coastal current in the model along the west bank of the strait from October to April the following year with it being the strongest and widest in January [*Chai et al.*, 2001]. *Lee and Chao* [2003] used similar annual distribution of transport as their open boundary condition in the Taiwan Strait for their East China Sea circulation model with the minimum northward transport of 0.5 Sv in December–January–February to the maximum northward transport of 2.4 Sv in August–September. On the basis of 8 ADCP cruises conducted between August 1999 and May 2001 in the Penghu Channel, the major inflow region of the Taiwan Strait, *Jan and Chao* [2003] concluded that the seasonal transport through the Penghu Channel varies from 0.5 Sv in spring, to more than1.5 Sv in summer, and then decreases with time to nearly zero in late fall and winter.

[23] Net transport through the Karimata Strait (T_K) is the result of the open boundary condition from the POCM (see section K in Figure 3). It varies seasonally with southward outflow from October to March that reverses to northward inflow from April to September. The maximum outflow (inflow) occurs in January (July) at about 3.0 (2.5) Sv. Model calculated transport through section M (T_M, mostly through the Mindoro Strait) has a seasonal variation almost opposite to the transport through the Karimata with southward outflows from April to November and northward inflows from December to March the following year, which appears to agree with the seasonal circulation pattern at the 23.0 kg m^{-3} δ_θ surface [*Chu and Li*, 2000]. Annual mean of T_M and T_K are 0.6 and 0.1 Sv southward, respectively. The former is about one third of the annual mean transport through the Luzon Strait (2.0 Sv), while the latter only amounts to 5%. Both the Karimata and the Taiwan Strait are shallow, and the transport through which is in phase with the monsoon winds with the maximum northward transport in summer. River input and the surface net fresh water flux (Evaporation minus Precipitation) are two orders smaller than the transport through the Luzon or the Taiwan Strait.

[24] In order to achieve an equilibrium solution, exact mass balance is required in the model such that T_L would need to be approximately $T_T + T_K + T_M$ (i.e., 2.3 Sv). Thus T_L shown in Figure 8 is about 10% underestimated. This error is likely resulted from both the horizontal and vertical interpolation, especially where the bottom topography changes abruptly such as in the Luzon Strait. Even at 2.3 Sv, T_L obtained from this model is still smaller than the estimate of *Qu* [2000]. *Qu* [2000], however, uses 0.5° × 0.5° resolution in his dynamic calculation, which could lead to considerable error given the complex alternating inflow/outflow pattern in the Luzon Strait (see section 4b below).

4.2. Inflows and Outflows in the Luzon Strait

[25] The net transport seen in Figure 8 does not completely reflect the complex circulation pattern in the Luzon Strait. There are three trenches in the Luzon Strait. From Luzon to Taiwan, they are the Babuyan, the Balintang, and the Bashi Channel (Figure 10a). Model results depict interleaving inflows and outflows in the strait. Inflows occur next to the Luzon coast, in Balintang Channel, and over the rise between the Bashi and the Balintang Channel, majority of which is in the Balintang Channel. Two segments of weak outflow exist between the three segments of inflow, while the strongest outflow occurs in the Bashi Channel. Inflows appear to be year-round. Even in the months of net outflow (Figure 10b), there are relatively weaker inflows in the mid section of the strait.

[26] From January to October, the core of the inflow shifts northward from the Babuyan Channel to the northern Balintang Channel. Inward speed is larger in fall and winter but smallest in spring. On the other hand, the outflow south of Taiwan weakens from January to October. It is the combination of the seasonal transition of the inflows and outflows that gives rise to the temporal variation of the net flux seen in Figure 8. In August and September of 1994, Chinese scientists aboard 4 research vessels surveyed the Luzon Strait and nearby regions using shipboard CTD and ADCP. Three pairs of interleaving inflows and outflows were found in the Luzon Strait [*Xu and Su*, 1997]. The present model results compare favorably with the observations in terms of direction and location of the alternating flow pattern (Table 2).

4.3. Circulation Patterns in the Northeastern SCS

[27] Kuroshio intrusion plays an important dynamical role in the northern SCS. *Fang et al.* [1998] suggested that

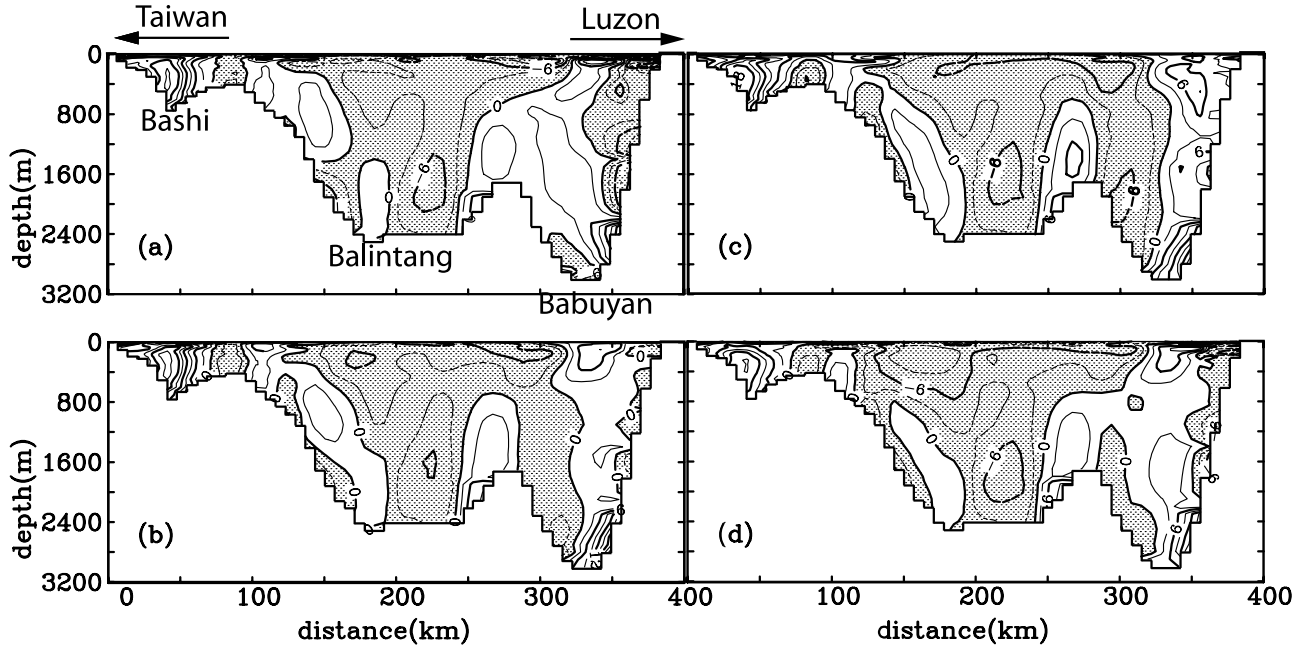

Figure 10. Velocity perpendicular to the section L in (a) January, (b) April, (c) July, and (d) October. Contour interval is 3 cm s^{-1}, and negative values are shaded. Positive (negative) velocities correspond to eastward (westward) flows.

the intruded Kuroshio splits into the anticyclonic current loop west of the Luzon Strait, the westward South China Sea Branch of the Kuroshio (SCSBK) on the slope, and the cyclonic eddy west of the Luzon Island (see Figure 2). In the model, the inflow of the Kuroshio is in the form of a loop current most time of the year except during the fall (Figure 11), entering on the south side of the strait and exiting on the north side. The loop has the widest north-south extension in winter (Figure 11a) corresponding to the most southern location of the inflow at the time (as seen in Figure 10a). In spring and summer, there is an anticyclonic eddy embedded in the current loop. When the inflow through the Luzon Strait shifts northward during the fall, the current loop becomes disintegrated and the anticyclones eddy emerges as the independent feature between Dongsha and Taiwan. Both the current loop and the anticyclonic eddy are associated with a warm center that is clearly visible even at 200-m depth with temperature 1°C warmer than the surrounding water (not shown).

[28] The cyclonic Luzon Eddy is most apparent in April (Figure 11b). In summer, there is a westward current on the slope with a mixture of waters from the intruded Kuroshio and from the interior SCS (Figure 11b). Furthermore, warm water leaks onto the shelf intermittently as evidenced by the two separate warm pools just outside of the shelf break, which mimics the schematics of *Fang et al.* [1998] (see Figure 2). The SCSBK occurs most apparently in the fall, flowing southwestward following approximately the 1000-m isobath (Figure 11d). The SCSBK is associated with a visible, warm band that extends across the entire northern slope, agreeing with the hydrographic analysis of *Shaw* [1991].

[29] One reason mentioned earlier is that the westward invasion of the modified Kuroshio water compensates the water loss in the western SCS due to summertime offshore Ekman transport. On the other hand, the formation of the SCSBK in fall can also be explained dynamically on the basis of the Kuroshio morphology near the Luzon Strait. Derived by *Hurlburt and Thompson* [1980], the equation that describes the path of the current loop in a simplified β plane, frictionless, steady state, reduced gravity model, is given as the following.

$$\sin\theta\frac{d\theta}{dy} = -\frac{\beta}{v_c}y + \frac{v_{co}}{v_c}\sin\theta_o\left.\frac{d\theta}{dy}\right|_{y=0} \quad (1)$$

where v_c is the speed at the core of the current, and θ is the angle between the velocity vector and the positive x axis as

Table 2. Comparison of the Modeled and Observed Inflows and Outflows in the Luzon Strait[a]

	Model Results (15 Aug. to 15 Sept.)			Observations in Aug.–Sept. 1994 [*Xu and Su*, 1997]		
Current Zones	Direction	Width	Depth	Direction	Width	Depth
1	W	19.0°–19.4°N	0 ~ 700 m	W	19.0°–19.3°N	0 ~ 500 m
2	E	19.4°–19.7°N	200 ~ 400 m	E	19.3°–19.9°N	0 ~ 500 m
3	W	19.7°–20.9°N	0 ~ 700 m	W	19.9°–20.4°N	0 ~ 300 m
4	E	20.9°–21.1°N	0 ~ 700 m	E	20.4°–21.0°N	0 ~ 400 m
5	W	21.1°–21.3°N	0 ~ 600 m	W	21.0°–21.6°N	0 ~ 600 m
6	E	21.3°–22.0°N	0 ~ bottom	E	21.6°–22.2°N	0 ~ bottom

[a]Here, W is westward (inward) flows, and E is eastward (outward) flows.

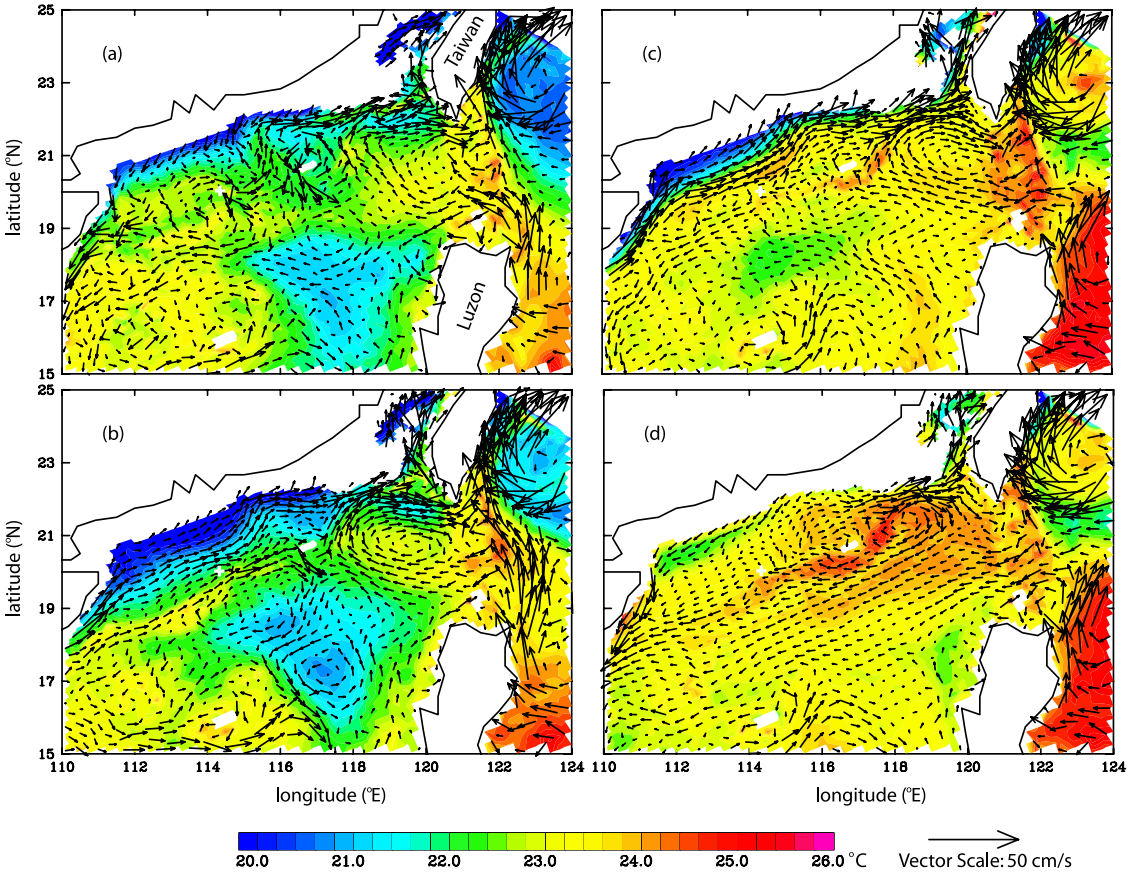

Figure 11. The 50-m temperature and velocity in (a) January, (b) April, (c) July, and (d) October.

seen in Figure 12. At the entrance ($y = 0$), $v_c = v_{co}$ and $\theta = \theta_o$. In this case, $\theta_o \approx \pi$, and thus the second term on the right hand side is nil. If one further assumes that v_c is constant, equation (1) can be integrated and becomes

$$1 + \cos\theta = \frac{\beta}{2v_c} W_L^2 \qquad (2)$$

[30] Equation (2) can be solved for W_L and the current loop exists only when $W_L < W_o$. Figure 13 shows the velocity distribution in the Luzon Strait, vertically averaged in the upper 200 m. The major portion of the inflow appears in the Balintang Channel. The core of the inflow shifts northward from January to October. Meanwhile, the core velocity, v_c, also varies. Table 3 lists the values corresponding to the inflow in January, April, July, and October and the calculated W_L assuming $\theta = 0$ as the outflow angle. W_L is less than W_o in January, April, and July, whereas it is greater than W_o in October. This suggests that the current loop can exists in January, April, and July, but not in October. In October, a large portion of the intruded Kuroshio water moves westward on the slope as the SCSBK, and a small portion moves onto the shelf to feed an eastward current that eventually becomes the Taiwan Warm Current.

4.4. The South China Sea Warm Current (SCSWC)

[31] In this paper, the name SCSWC is used exclusively for the eastward flowing warm current along the continental shelf break in the winter. Although eastward flows exist year around near the shelf break, water mass characteristics are rather different between the winter and the summer months [*Shaw*, 1991].

[32] The SCSWC appears to be weak and disorganized at the surface. At 50 m the SCSWC is sustained from November to February the following year. It is found near the shelf break with a width of 100 km, length of 600 km (from 114° to 120°E), and maximum velocity of ~30 cm s^{-1}

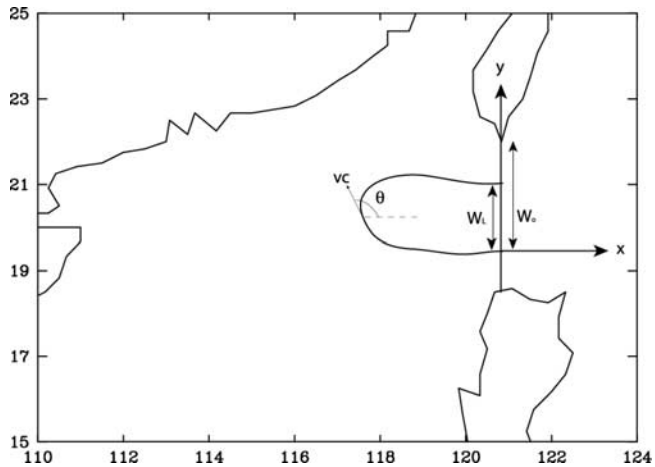

Figure 12. Schematic of the Kuroshio intrusion and the anticyclonic current loop west of the Luzon Strait.

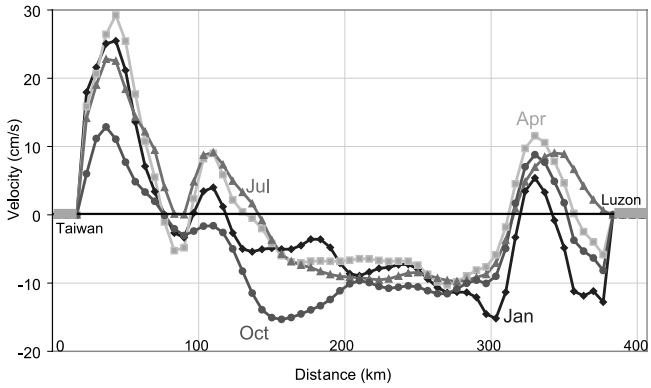

Figure 13. Seasonal variation of the velocity in the Luzon Strait, vertically averaged in the upper 200 m. Positive (negative) values correspond to eastward (westward) flows.

(Figure 11a). Temperature of the SCSWC is about 1°–2°C warmer than the surrounding water. These results agree well with the observed characteristics of the SCSWC [*Guan*, 1978, 1985; *Guo et al.*, 1985; *Huang and Zheng*, 1995].

[33] The most striking feature of the SCSWC is that it is against the prevailing wind. A simple diagnostics can reveal the presence of upwelling on the upper slope and the importance of both the barotropic and the baroclinic gradient in the formation of the SCSWC.

$$-fv = -g\frac{\partial \eta}{\partial x} - \frac{\partial \varphi}{\partial x} + \frac{\partial \tau_x}{\partial z} \tag{3a}$$

$$fu = -g\frac{\partial \eta}{\partial y} - \frac{\partial \varphi}{\partial y} + \frac{\partial \tau_y}{\partial z} \tag{3b}$$

where (u, v) are velocity components in the offshore and alongshore direction (see the local coordinate in Figure 12), η is the surface elevation, and $\varphi = \int_z^0 (g\rho')/\rho_o dz$ is the dynamic height. Assuming (1) constant wind stress (τ_o) in the alongshore direction and zero wind stress in the offshore direction, (2) linear bottom stress (τ_{bx}, τ_{by}) = γ (u, v), and (3) there is no alongshore pressure gradient, the diagnostic equations for the vertically averaged velocity in the offshore and alongshore direction $(\bar{u}, \bar{v})$ are

$$\bar{u} = \frac{f}{(\gamma/H)^2 + f^2}\left(\frac{\tau_o}{H}\right) - \frac{g(\gamma/H)}{(\gamma/H)^2 + f^2}\frac{\partial n}{\partial x} - \frac{(\gamma/H)}{(\gamma/H)^2 + f^2}\frac{1}{H}\int_{-H}^{0}\frac{\partial \varphi}{\partial x}dz \tag{4a}$$

$$\bar{v} = \frac{\gamma/H}{(\gamma/H)^2 + f^2}\left(\frac{\tau_o}{H}\right) + \frac{gf}{(\gamma/H)^2 + f^2}\frac{\partial n}{\partial x} + \frac{f}{(\gamma/H)^2 + f^2}\frac{1}{H}\int_{-H}^{0}\frac{\partial \varphi}{\partial x}dz. \tag{4b}$$

[34] The alongshore wind plays an important role in the dynamic balance in the offshore direction. For typical values of $\gamma = 2 \times 10^{-4}$ m s^{-1}, $f = 5 \times 10^{-5}$ s^{-1}, H = 100 m, and $\tau_o = 0.1$ N m^{-2}, the first term on the RHS of equation (4a), $\bar{u}_1 = (\tau_o/H) \bullet f/((\gamma/H)^2 + f^2)$, estimated at ~ 0.025 m s^{-1} shoreward, while the second term is ~ 0.006 m s^{-1}. The wind-driven Ekman transport, $\bar{u}_1$, brings the warmer and less saline surface water onshore in case of northeasterly wind. Its gradient, $(\partial \bar{u}_1/\partial x = \tau_o(\partial H/\partial x \bullet ((\gamma/H)^2 - f^2)/((\gamma/H)^2 + f^2))$, however, is positive for $\tau_o < 0$ (i.e., northeasterly wind), which leads to upwelling on the upper slope. The upwelling results in a band of high-salinity and low-temperature surface water on the upper slope, which separates the band of warm and less saline water on the shelf from its offshore origin, as shown in Figures 14b and 14c.

[35] On the other hand, pressure gradient terms are dominant in the alongshore direction, with the three terms on the RHS of equation (4b) estimated at $\sim$0.01, $\sim$0.2, and $\sim$0.1 m s^{-1}, respectively. The direct wind-driven current is westward ($\bar{v}_1 < 0$). However, $\bar{v} > 0$ occurs where there is positive barotropic and/or baroclinic pressure gradient. It is therefore obvious that there exists an eastward flowing current (the SCSWC) on the offshore side of the shelf break with sea level and density distributions shown in Figures 14a–14c. Since it is against the prevailing wind direction, the current is strongest below the surface at about 50-m depth.

5. Summary

[36] The Princeton Ocean Model has been configured for the SCS with unprecedentedly high resolution in the northern shelf/slope region of the SCS. The model has been integrated forward in time for 20 years with climatological monthly forcing, and the upper ocean has attained a quasi-equilibrium annual cycle. The model shows the seasonally alternating basin-wide circulation, the Kuroshio intrusion and the associated anticyclonic current loop west of the Luzon Strait, and the SCSWC in the winter, all in good agreement with observations.

[37] The upper layer of the SCS is driven primary by the seasonal monsoon wind. During winter the northeasterly monsoon drives the southwestward and southward currents along the China and Vietnam coasts, whereas during summer these currents reverse under the southwesterly monsoon. Furthermore, the model reproduced the twin cyclonic eddies encompassed by a cyclonic gyre in the southern basin during winter. There also exists a cyclonic eddy in the northern basin, which is separated from the south cyclonic gyre by an anticyclonic eddy off the coast of Vietnam. In summer, the circulation in the southern basin changes to anticyclonic, while the circulation remains cyclonic in the northwestern SCS. These seasonal basin wide features agree well with the schematic of *Fang et al.* [1998]. Finally, the model-simulated seasonal sea surface anomaly patterns agree with satellite altimetry data, and they are dynamically consistent with the basin wide circulation.

Table 3. Characteristic Values Associated With the Kuroshio Inflow in the Luzon Strait and the Calculated Inertial Distance W_L

	W_o, km	v_c, cm/s	B, 1/m s	WL, km
January	288	15.2	2.1456×10^{-11}	168
April	254	10.3	2.1428×10^{-11}	139
July	202	9.8	2.1387×10^{-11}	135
October	138	15.3	2.1344×10^{-11}	169

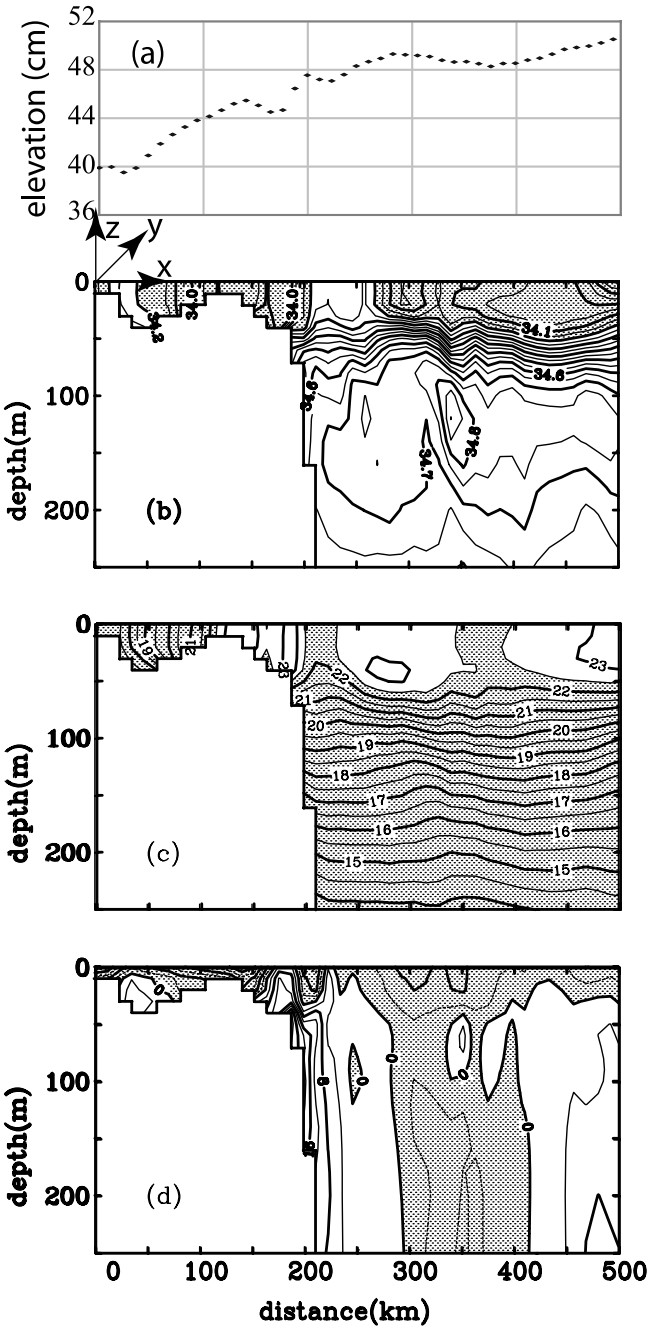

Figure 14. January distributions of (a) sea level, (b) salinity, (c) temperature, and (d) velocity (see Figure 2 for the location of the cross section W). Contour interval is 0.05 for salinity, 0.5°C for temperature, and 4 cm s^{-1} for velocity, respectively. Shaded areas correspond to salinity >34.1 in Figure 14b, temperature <22.5°C in Figure 14c, and velocity <0 in Figure 14d, which represent the westward flows.

[38] Net transport through the Luzon Strait is ~2 Sv into the SCS on the annual average. It, however, exhibits a remarkable seasonal variation. From May to January, the net flow through the strait is from the Pacific into the SCS at an average of 3.3 Sv. More Kuroshio water reaches the western SCS at deep levels, especially during summer and fall. The seasonal variation in the net transport appears to be closely related to the east-west sea level difference between Vietnam coast and the Luzon Strait with an approximate 2-month delay. It is therefore concluded that the elevated net influx during the fall is to compensate the summertime coastal upwelling along the Vietnam and southern China coasts. From February to April, the net transport is from the SCS to the Pacific with a flux of 1.8 Sv.

[39] Although the net transport through the Luzon Strait varies, the Kuroshio enters the SCS year-round. The Kuroshio intrusion forms an apparent anticyclonic current loop west of the Luzon Strait most of the year except in the fall when the majority of the intruded Kuroshio flows westward to form the SCSBK spanning across the entire northern slope. On the other hand, the anticyclonic current loop has profound influences on the water properties on the northern shelf/slope region, especially during the northeasterly monsoon in the winter when the Ekman transport brings the warmer Kuroshio water onshore. As the Kuroshio water moves upslope, it induces an upwelling on the upper slope, and the associated barotropic and baroclinic pressure gradient supports the eastward SCSWC, against the prevailing wind. The modeled SCSWC appears near the shelf break from 115° to 120°E. It is about 100-km wide with a maximum velocity of ~30 cm s^{-1}, and it is sustained from November to February the following year.

[40] Since the SCSWC and the SCSBK exist on the continental slope and the slope is rather narrow off Vietnam and Luzon, it is often suspected that the results are subjected to the pressure gradient error in a sigma coordinate model such as POM. Numerical experiments using POM with a generalized vertical coordinate [*Mellor et al.*, 2002] and with more vertical levels are recommended for future studies in order to determine whether the pressure gradient error is significant. Second, the POCM is known to underestimate the eddy kinetic energy in the open ocean [*McClean et al.*, 1997] and the interaction between the open ocean eddies and the Kuroshio can produce transport variability on the order of 10 Sv [*Zhang et al.*, 2001]. Further investigation is needed to determine the degree of influence of the Kuroshio transport variability on the intrusion in the Luzon Strait and, subsequently, the circulation in the northern SCS, though *Metzger and Hurlburt* [2001] believe that Kuroshio transport does not affect Kuroshio penetration into the SCS.

[41] **Acknowledgments.** The present study was supported by grants from Office of Naval Research (N00014-97-1-1075) and National Science Foundation of China (90211021). Also, we thank the two anonymous reviewers for their comments and suggestions.

References

Blumberg, A. F., and G. L. Mellor (1987), A description of a three-dimensional coastal ocean circulation model, in *Three-Dimensional Coastal Ocean Models*, *Coastal Estuarine Stud.*, vol. 4, edited by N. Heaps, pp. 1–16, AGU, Washington, D. C.

Chai, F., H. Xue, and M. Shi (2001), The study of transport in the Taiwan Strait (in Chinese with English abstract), in *Oceanography in China*, vol. 13, edited by H. Xue, pp. 168–177, China Ocean, Beijing.

Chao, S.-Y., P.-T. Shaw, and J. Wang (1995), Wind relaxation as a possible cause of the South China Sea Warm Current, *J. Oceanogr.*, *51*, 111–132.

Chu, P. C., and R. Li (2000), South China Sea isopycnal surface circulation, *J. Phys. Oceanogr.*, *30*, 2419–2438.

Chu, P. C., N. L. Edmons, and C. Fan (1999), Dynamical mechanisms for the South China Sea seasonal circulation and thermohaline variabilities, *J. Phys. Oceanogr.*, *29*, 2971–2989.

Csanady, G. T. (1978), The arrested topographic wave, *J. Phys. Oceanogr.*, *8*, 47–82.
Fang, G.-H., W.-D. Fang, Y. Fang, and K. Wang (1998), A survey of studies on the South China Sea upper ocean circulation, *Acta Oceanogr. Taiwan.*, *37*, 1–16.
Farris, A., and M. Wimbush (1996), Wind-induced Kuroshio intrusion into the South China Sea, *J. Oceanogr.*, *52*, 771–784.
Guan, B.-X. (1978), The warm current in the South China Sea: A current against the wind in winter in the open sea off Guang Dong Province (in Chinese), *Oceanol. Limnol. Sin.*, *9*, 117–127.
Guan, B.-X. (1985), Some feature of the temporal and spatial distribution of the "counter-wind" current in northern South China Sea in winter (in Chinese), *Oceanol. Limnol. Sin.*, *16*, 429–438.
Guo, Z.-X., T.-H. Yang, and D.-Z. Qiu (1985), South China Sea Warm Current and a southwestward current on its right side in winter (in Chinese), *Trop. Oceanol.*, *4*, 1–9.
Hu, J., H. Kawamura, H. Hong, and Y. Qi (2000), A review on the currents in the South China Sea: Seasonal circulation, South China Sea Warm Current and Kuroshio intrusion, *J. Oceanogr.*, *56*, 607–624.
Huang, Q.-Z., and Y.-R. Zheng (1995), Currents in the northeastern South China Sea and Bashi Channel in March 1992, in *Proceedings of Symposium of Marine Sciences in Taiwan Strait and its Adjacent Waters*, pp. 15–19, China Ocean Press, Beijing.
Hurlburt, H. E., and J. D. Thompson (1980), A numerical study of Loop Current intrusions and eddy shedding, *J. Phys. Oceanogr.*, *10*, 1611–1651.
Jan, S., and S.-Y. Chao (2003), Seasonal variation of volume transport in the major inflow region of the Taiwan Strait: The Penghu Channel, *Deep Sea Res., Part II*, *50*, 1117–1126.
Lau, N.-C., and K.-H. Lau (1992), Simulation of the Asian summer monsoon in a 40-year experiment with a general circulation model, in *East Asia and Western Pacific Meteorology and Climate*, edited by W. J. Kyle and C. P. Chang, pp. 49–56, World Sci., River Edge, N. J.
Lee, H.-J., and S.-Y. Chao (2003), A climatological description of circulation in and around the East China Sea, *Deep Sea Res., Part II*, *50*, 1065–1084.
Li, L., and B.-Y. Wu (1989), A Kuroshio loop in the South China Sea?—On circulations of the northeastern South China Sea (in Chinese), *J. Oceanogr. Taiwan Strait*, *8*, 89–95.
Li, L., W. D. Nowlin Jr., and J. Su (1998), Anticyclonic rings from the Kuroshio in the South China Sea, *Deep Sea Res., Part I*, *45*, 1469–1482.
Li, R.-F., Q.-Z. Huang, and W.-Z. Wang (1994), Numerical simulation of the upper layer currents in the South China Sea (in Chinese), *Acta Oceanol. Sin.*, *16*(4), 13–22.
Liu, K., J. Ma, J. Xu, G. Han, and Z. Fan (2001), Sea surface height anomaly and geostrophic circulation variations in the South China Sea from TOPEX/Poseidon altimetry (in Chinese with English abstract), in *Oceanography in China*, vol. 13, edited by H. Xue et al., pp. 231–240, China Ocean, Beijing.
McClean, J. L., A. J. Semtner, and V. Zlotnicki (1997), Comparisons of mesoscale variability in the Semtner-Chervin 1/4° model, the Los Alamos Parallel Ocean Program 1/6o model, and TOPEX/Poseidon data, *J. Geophys. Res.*, *102*, 25,203–25,226.
Mellor, G. L., S. Hakkinen, T. Ezer and R. Patchen (2002), A generalization of a sigma coordinate ocean model and an intercomparison of model vertical grids, in *Ocean Forecasting: Conceptual Basis and Applications*, edited by N. Pinardi and J. D. Woods, pp. 55–72, Springer, New York.
Metzger, E. J., and H. E. Hurlburt (1996), Coupled dynamics of the South China Sea, the Sulu Sea, and the Pacific Ocean, *J. Geophys. Res.*, *101*, 12,331–12,352.
Metzger, E. J., and H. E. Hurlburt (2001), The nondeterministic nature of Kuroshio penetration and eddy shedding in the South China Sea, *J. Phys. Oceanogr.*, *31*, 1712–1732.
Nitani, H. (1972), Beginning of the Kuroshio, in *Kuroshio, Physical Aspects of the Japan Current*, edited by H. Stommel and K. Yashida, pp. 129–163, University of Wash., Seattle.
Perry, G. D., P. B. Duffy, and N. L. Miller (1996), An extended data set of river discharges for validation of general circulation models, *J. Geophys. Res.*, *101*, 21,339–21,349.
Qu, T. (2000), Upper layer circulation in the South China Sea, *J. Phys. Oceanogr.*, *30*, 1450–1460.
Qu, T., H. Mitsudera, and T. Yamagata (2000), Intrusion of the North Pacific waters into the South China Sea, *J. Geophys. Res.*, *105*, 6415–6424.
Shaw, P.-T. (1991), The seasonal variation of the intrusion of the Philippine Sea Water into the South China Sea, *J. Geophys., Res.*, *96*, 821–827.
Shaw, P.-T., and S.-Y. Chao (1994), Surface circulation in the South China Sea, *Deep Sea Res., Part I*, *41*, 1663–1683.
Shi, M., M. Jiang, F. Chai, and H. Xue (2001), Formation of the Zhongsha southern anticyclonic circulation and the circulation in the deep basin of the South China Sea (in Chinese with English abstract), in *Oceanography in China*, vol. 13, edited by H. Xue et al., pp. 90–104, China Ocean, Beijing.
Wu, C.-R., P.-T. Shaw, and S.-Y. Chao (1999), Assimilating altimetric data into a South China Sea Model, *J. Geophys. Res.*, *104*, 28,987–30,005.
Wyrtki, K. (1961), Physical oceanography of the southeast Asian waters, Scientific results of marine investigations of the South China Sea and the Gulf of Thailand, *NAGA Rep. 2*, 195 pp., Scripps Inst. of Oceanogr., La Jolla, Calif.
Xu, J.-P., and J.-L. Su (1997), Hydrological analysis on the intrusion of the Kurushio into the South China Sea: Observational results during the cruise from August to September in 1994 (in Chinese), *Trop. Oceanol.*, *16*, 1–23.
Xue, H., F. Chai, N. R. Pettigrew, D. Xu, and M. Shi (2000), Upper ocean circulation in the northern South China Sea, paper presented at Second International Ocean and Atmosphere Conference, Chin.-Am. Oceanic and Atmos. Assoc., Taipei.
Zhao, H. (1990), *Evolution of the Pearl River Estuary* (in Chinese), 357 pp., China Ocean, Beijing.
Zhang, D., T. N. Lee, W. E. Johns, C.-T. Liu, and R. Zantopp (2001), The Kuroshio east of Taiwan: Modes of variability and relationship to interior ocean mesoscale eddies, *J. Phys. Oceanogr.*, *31*, 1054–1074.
Zhong, L. (2001), The circulation in the northern South China Sea, Ph. D. thesis, Fla. State Univ., Tallahassee.

F. Chai, N. Pettigrew, D. Xu, and H. Xue, School of Marine Sciences, University of Maine, Orono, ME 04469-5741, USA. (hxue@maine.edu)
M. Shi, Ocean University of China, Qingdao 266003, China.
J. Xu, Second Institute of Oceanography, Hangzhou 310012, China.